Modeling, Analysis, and Design of Graphene Nano-Ribbon Interconnects

Chuan Xu, *Student Member, IEEE*, Hong Li, *Student Member, IEEE*, and Kaustav Banerjee, *Senior Member, IEEE*

***Abstract*—Graphene nanoribbons (GNRs) are considered as a prospective interconnect material. A comprehensive conductance and delay analysis of GNR interconnects is presented in this paper. Using a simple tight-binding model and the linear response Landauer formula, the conductance model of GNR is derived. Several GNR structures are examined, and the conductance among them and other interconnect materials [e.g., copper (Cu), tungsten (W), and carbon nanotubes (CNTs)] is compared. The impact of different model parameters (i.e., bandgap, mean free path, Fermi level, and edge specularity) on the conductance is discussed. Both global and local GNR interconnect delays are analyzed using an RLC equivalent circuit model. Intercalation doping for multilayer GNRs is proposed, and it is shown that in order to match (or better) the performance of Cu or CNT bundles at either the global or local level, multiple zigzag-edged GNR layers along with proper intercalation doping must be used and near-specular nanoribbon edge should be achieved. However, intercalation-doped multilayer zigzag GNRs can have better performance than that of W, implying possible application as local interconnects in some cases. Thus, this paper identifies the on-chip interconnect domains where GNRs can be employed and provides valuable insights into the process technology development for GNR interconnects.**

***Index Terms*—Armchair graphene nanoribbon (ac-GNR), carbon nanotube (CNT), conductance, delay modeling, graphene nanoribbon (GNR), intercalation doping, specularity, very large scale integration (VLSI) interconnects, zigzag GNR (zz-GNR).**

I. Introduction

GRAPHENE nanoribbons (GNRs) have been recently proposed as one of the potential candidate materials for both transistors [1] and interconnects [2]–[4]. GNRs are obtained by patterning graphene, which is a flat monolayer of carbon atoms tightly packed into a 2-D honeycomb lattice, and is a basic building block of carbon nanotubes (CNTs), GNRs, graphite, etc. [5], as shown in Fig. 1.

A. Basic Properties

Both GNRs and CNTs can conduct much larger current densities than Cu (a traditional interconnect material), due to their strong sp^2 hybridized bonds, and the absence of severe reliability problems that plague Cu, particularly for future interconnect geometries [7]–[11]. The thermal conductivities of GNRs and CNTs are also much larger than that of Cu [14]–[16]. Moreover, compared to Cu, both GNRs and CNTs have large carrier mean free paths (MFPs), which lead to large electrical conductance [18]–[20]. However, GNRs are believed to be more controllable from a fabrication point of view. This is due to the planar nature of graphene, which can be patterned using high-resolution lithography. The properties of GNRs, Cu, single-walled CNTs (SWCNTs), and multiwalled CNTs (MWCNTs), relevant to interconnect applications, are listed in Table I.

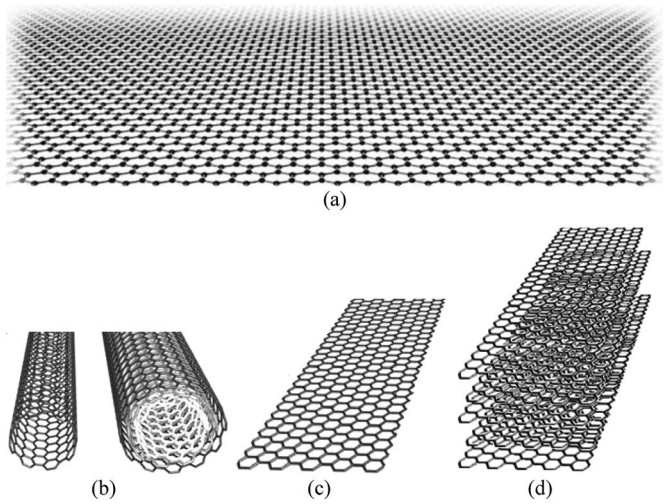

Fig. 1. Lattice structures of (a) graphene [5], (b) carbon nanomaterials based on graphene [left: single-walled; right: multiwalled CNTs (rolled graphene sheets)] [6], (c) monolayer GNR (patterned graphene sheet), and (d) multilayer GNR (patterned graphite).

TABLE I
PROPERTIES OF GRAPHENE/GNRs, Cu, AND CNTs RELEVANT TO VLSI INTERCONNECTS

		Cu	SWCNT	MWCNT	Graphene or GNR
Max current density (A/cm^2)		10^7	$>10^9$ [9]	$>10^9$ [10]	$>10^8$ [11]
Melting point (K)		1356	3773 (graphite)		
Tensile strength (GPa)		0.22	22.2±2.2 [12]	11-63 [13]	-
Thermal conductivity ($\times 10^3$ W/mK)		0.385	1.75-5.8 [14]	3 [15]	3-5 [16],[17]
Mean free path (nm) @ room temperature		40	$>10^3$ [18]	2.5×10^4 [19]	1×10^3 [20]
Status of fabrication techniques	Films / Horizontal wires	mature	not known	nascent stage [21]	known but immature [22]
	Vertical vias	mature	nascent stage [23]	known [6]	not known

Manuscript received December 1, 2008; revised April 27, 2009. Current version published July 22, 2009. This work was supported by the National Science Foundation under Grant CCF-0811880. The review of this paper was arranged by Editor M. Reed.

The authors are with the Department of Electrical and Computer Engineering, University of California, Santa Barbara, CA 93106 USA (e-mail: chuanxu@ece.ucsb.edu; hongli@ece.ucsb.edu; kaustav@ece.ucsb.edu).

Color versions of one or more of the figures in this paper are available online at http://ieeexplore.ieee.org.

Digital Object Identifier 10.1109/TED.2009.2024254

To comprehend the outstanding electrical and thermal properties of GNRs and CNTs, it is important to understand the electronic band structure of graphene. According to the tight-binding model [24], graphene is a semimetal or a zero-gap semiconductor, with a linear energy spectrum of $E = \pm h v_f \Delta k / 2\pi$ near the Dirac points [Fig. 2(a)], where Δk is the distance from the Dirac points to any point in the k space, h is Planck's constant, $v_f = \sqrt{3}\pi\gamma a/h = 10^6$ m/s is the Fermi velocity, where $\gamma = 3$ eV is the overlap integral between nearest neighbor π-orbitals, and $a = 0.246$ nm is the lattice constant [25]. Due to the linear energy dispersion near the Dirac points, the charge carriers in graphene mimic relativistic particles with constant magnitude of v_f, which are called massless Dirac Fermions. Due to the limited width of GNRs, they are confined 1-D structures: wave function vanishes at two edges. Thus, the transverse wave vector in GNR is quantized with separation of π/w ($w = i\lambda/2$ or $k = i\pi/w$, where i is an integer, and λ is the wave length), where w is the width of the GNR. As a result, armchair GNRs (ac-GNRs) [Fig. 2(b)] can be either metallic (the transverse wave vector with respect to the Dirac point, $\Delta k_{\text{transverse}} = n\pi/w$, where n is an integer; note that when $n = 0$, $\Delta k_{\text{transverse}} = 0$, implying that the zeroth subbands pass through the Dirac points) or semiconducting [$\Delta k_{\text{transverse}} = (n + 1/3)\pi/w$ or $\Delta k_{\text{transverse}} = (n - 1/3)\pi/w$], depending on the number (N) of hexagonal carbon rings across the width: metallic when $N = 3m - 1$ and semiconducting when $N = 3m$ or $3m + 1$ [Fig. 2(d) and (e)] [26]. In comparison, zigzag GNRs (zz-GNRs) are always metallic and independent of N. However, the electronic states of zz-GNRs are more complicated. Particularly, the zz-GNRs have the "dispersionless band" or "zero-mode," which originates from the edge states [26]–[28] [Fig. 2(f)]: almost flatband appears within the region of $2\pi/3 < |ka| \leq \pi$. Note that for the same w, the N of ac-GNRs is approximately $\sqrt{3}$ times larger than the N of zz-GNRs due to the nature of the honeycomb lattice. It should also be noted that the band structure of the monolayer graphene can be strongly affected by the substrate (e.g., SiO_2 substrate with O-termination and without H-passivation) [29]. It is assumed in this paper that the graphene is deposited onto a proper substrate so that the tight-binding model is valid. Furthermore, for the case of multilayer GNRs, the substrate has negligible impact on the layers that are above the first few layers.

B. GNR Fabrication Methods

As mentioned earlier, the interest in GNRs is mainly due to their deemed patternability to produce metallic or semiconducting structures on demand. Various methods for fabricating GNRs are being pursued, but difficulties also exist in those methods. Carbon films have been demonstrated in dynamic random access memory trench capacitors using the chemical vapor deposition method [30], but the grown films are not single-crystal graphene films with ultrahigh electrical conductivity. Although thermal decomposition of single-crystal (0001) 6H-SiC or 4H-SiC can produce thin graphene films [31], [32], this approach requires single-crystal substrates and high temperatures, which is not suitable for interconnects due to the relatively low back-end thermal budget (~400 °C) in integrated circuit fabrication technologies. Graphene can also be mechanical exfoliated from graphite and deposited onto an insulating substrate [33], but this approach is uncontrollable for massive fabrication. In [22] (Fig. 3), graphene is segregated by dissolving carbon in a Ni substrate at high temperatures, covering with a silicone film, and then transferring to a desired substrate. The Ni substrate can be subsequently removed to allow GNR wire and contact formation through patterning. Similarly, graphene can be deposited onto copper (Cu) foils (which can be removed later) and transferred to insulating substrates [34]. While these approaches are more suitable for interconnect applications than the previous three approaches, they still require further investigation.

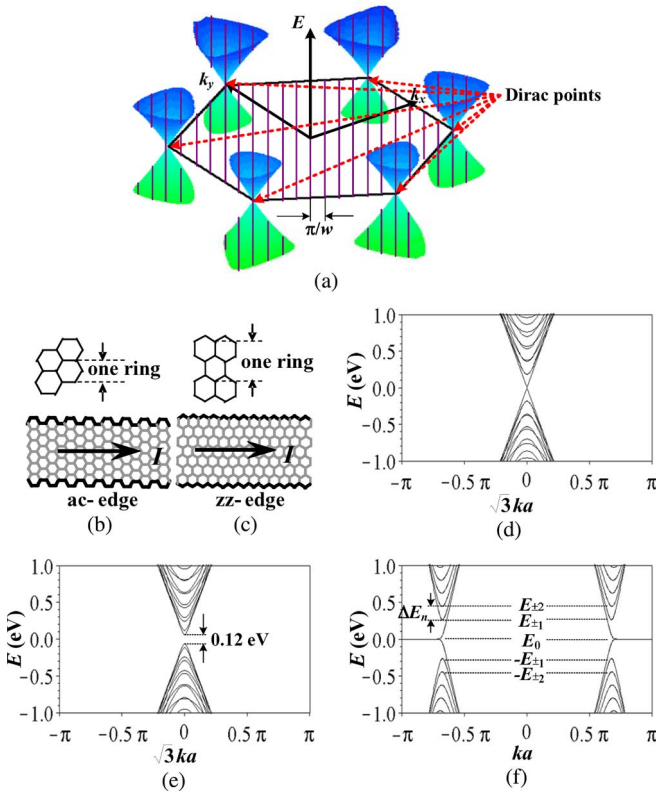

Fig. 2. (a) Band structure of graphene forming hexagonal cones in the vicinity of the Dirac points. Schematic view of (b) ac-GNR and (c) zz-GNR. Band structures of (d) metallic ac-GNR ($N = 44$), (e) semiconducting ac-GNR ($N = 45$), and (f) zz-GNR ($N = 26$) of similar width (11 nm). N is the number of hexagonal carbon rings across the width of the GNR, and a is the lattice constant ($a = 0.246$ nm). In (f), the subscript "E" indicates the subband index, while "±" indicates a degeneracy of 2. Note that $k_B T$ is much less than ΔE_n (the difference in energy between any adjacent subbands).

C. Fundamental Issues in GNRs and the Focus of This Paper

In addition to the fabrication challenges, several fundamental issues also exist in GNRs. First, GNRs have edge scattering, which reduces the effective MFP, while CNTs have no such issue. Second, while monolayer graphene has large MFP and conductivity, multilayer graphene turns to graphite and has much lower conductivity per layer due to intersheet electron hopping [35]. The interaction between layers also leads to a modification of the band structure (0.04 eV of band overlap is

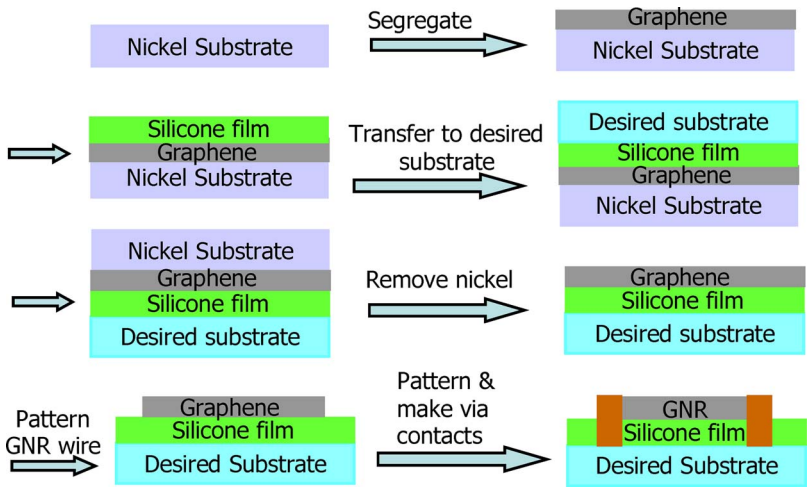

Fig. 3. Possible GNR interconnect fabrication strategy adapted from [22].

generated in neutral bulk graphite) [36]. In addition, zz-GNRs exhibit a nonzero bandgap [shown later in (17)] due to staggered sublattice potential from magnetic ordering once electron spin is considered [37], [38], which reduces the conductance. Hence, while various fabrication methods of GNRs are being pursued [2], [5], [22], [31]–[33], there is a critical need to evaluate the applicability of GNRs as very large scale integration (VLSI) interconnects and evaluate their performance in comparison to traditional metals (Cu and W) and CNTs. This will also provide guidance to the GNR interconnect fabrication processes.

In previous works [3], [4], the conductance of both metallic and semiconducting GNRs has been modeled and compared with Cu and SWCNTs. However, the assumption in [3] and [4] that ac-GNRs can be differentiated as metallic and semiconducting implies that N is fixed everywhere along the length (either $N = 3m - 1$ (metallic) or $N = 3m, 3m + 1$ (semiconducting), where m is an integer [3], [4]), which further implies very smooth (specular) edges of GNRs, and is against the complete diffusive edge assumption made in [3]. Although the above assumption is not against the complete specular-edge assumption in [4], theoretically, nanopatterning down to the accuracy of one atom is a formidable task from a practical point of view [26]. It should be noted that there are reports that graphene can be cut along certain crystallographic directions and potentially produce ac- or zz-GNRs with smooth edges using nanoparticles [39]. However, this approach is not controllable: neither the diameter of the particles (which determines the patterned slot width) nor the moving direction of the particles (which determines the patterned slot direction) can be accurately controlled.

Due to the high resistance of single graphene layers (discussed in Section III), it becomes necessary to use multiple graphene layers. Additionally, it has been shown that the conductivity of graphite can be enhanced by intercalation doping by exposure to dopant vapor (e.g., AsF_5 [40]–[42]). Recently, intercalation doping has been proposed to enhance the conductance of multilayer GNRs, and edge specularity effects for multilayer GNRs have been studied [43]. In this paper, details of both monolayer and multilayer GNRs are analyzed, and conductance as well as performance comparisons among GNRs, CNTs, Cu, and tungsten (W) are presented based on the interconnect geometry predicted in the International Technology Roadmap for Semiconductors (ITRS) 2007 [44] for both local and global level interconnects. An RLC delay model for GNR interconnects is also presented and used for comparative performance analysis.

II. Fundamental Physics and Models of GNR Conductance

The conductance of GNRs can be derived using the linear response (small voltage drop along the length) Landauer formula [45]: G_n, the conductance of the nth conduction mode (with consideration of spin) in a single GNR layer, is expressed as

$$G_n = 2q^2/h \cdot \int T_n(E)(-\partial f_0/\partial E)dE$$
$$f_0(E) = \{1 + \exp[(E - E_F)/k_BT]\}^{-1} \quad (1)$$

where q is the elementary charge, $T_n(E)$ is the transmission coefficient, $f_0(E)$ is the Fermi–Dirac distribution function, E_F is the Fermi level, k_B is Boltzmann's constant, and T is the temperature. The integration of (1) is from $|E_n|$ to $+\infty$ (for electrons) or from $-\infty$ to $-|E_n|$ (for holes), where E_n is the minimum (maximum) energy of the nth conduction (valence) subband. According to the simple tight-binding model (linear approximation near the Dirac point) [24], E_n of zz-GNRs can be expressed as [4]

$$E_0 = 0 \text{ and } |E_n| = (|n| + 1/2) \cdot hv_f/2w \qquad \text{for } n \neq 0 \quad (2)$$

where h is Planck's constant, $v_f = 10^6$ m/s is the Fermi velocity, and w is the width of the GNR. Fig. 4(a) shows E_n as a function of the index n for a particular zz-GNR, with $w = 30$ nm. $T_n(E)$ is determined by both edge scattering and scattering by defects and phonons. The edge scattering is schematically shown in Fig. 3(b), where $\cot\theta$ is the ratio of longitudinal (along the wire length) to transverse (across the wire width) velocities. θ can be expressed as a function of E_n and the total energy E of an electron or hole, which is shown in (25) and (26) in Appendix. Fig. 4(c) shows $\theta|_{E=E_F}$ ($E_F = -0.21$ eV,

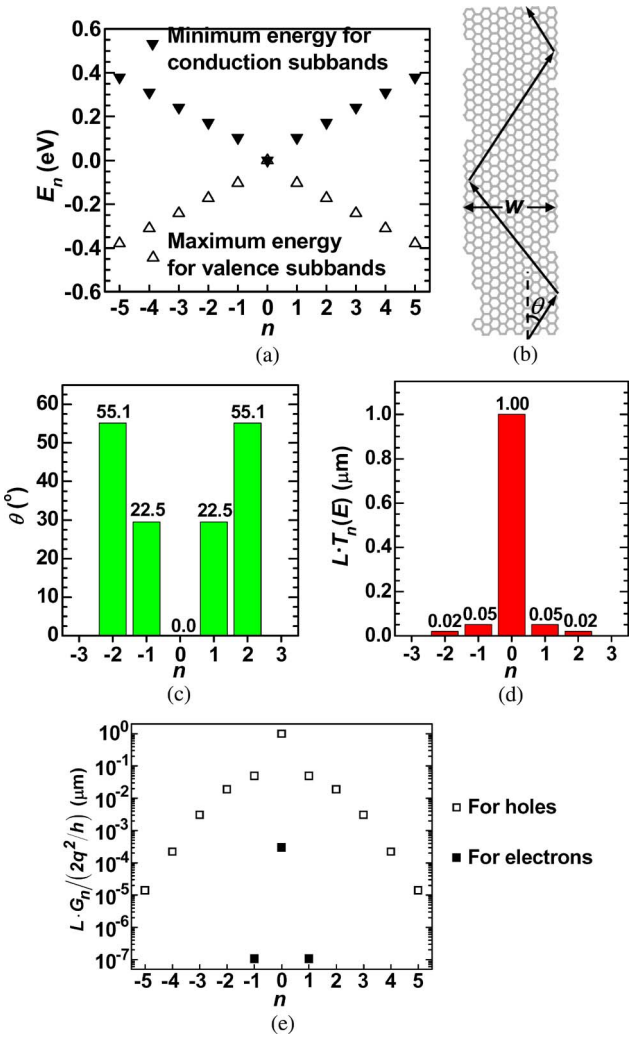

Fig. 4. Modeling of zz-GNR ($E_0 = 0$) conductance: (a) Minimum (maximum) energy of the nth conduction (valence) subband. (b) Schematic view of edge scattering in GNRs and the definition of θ. (c) θ for holes as a function of n at $E = E_F$. [Note that $|E_{\pm 3}| > |E_F|$, which implies that $E = E_F$ is not allowed for $n = \pm 3$ and $\theta|_{n=\pm 3, E=E_F}$ does not exist. See also (26) in Appendix.] (d) Transmission coefficient $T_n(E)$ in unit length for holes as a function of n at $E = E_F$. (e) Conductance in unit length of the nth conduction mode for both electrons and holes. Note that the negative values of n indicate degenerate subbands or conduction modes. GNR width $w = 30$ nm, $E_F = -0.21$ eV, and GNR length $L \gg l_D (= 1\ \mu\text{m})$.

which is below the Dirac point, implying p-type GNR) as a function of the subband or conduction mode index n. If complete diffusive edge is assumed, the transmission coefficient due to edge scattering can be expressed by "$w \cot\theta / L$," where $w \cot\theta$ is the distance that electrons/holes travel before hitting the edge, and L is the length of the GNR. On the other hand, due to scatterings by defects and phonons (not edge scattering), the transmission coefficient can be expressed by "$l_D \cos\theta / L$," where l_D is the MFP corresponding to such scattering. $l_D \cos\theta$ represents the average distance that an electron travels along the GNR longitude direction before collision. Hence, if complete diffusive edge is assumed, using the Matthiessen's rule, $T_n(E)$ can be obtained by

$$\frac{1}{T_n(E)} = 1 + \frac{L}{l_D \cos\theta} + \frac{L}{w \cot\theta} \approx \frac{L}{l_D \cos\theta} + \frac{L}{w \cot\theta}. \tag{3}$$

Here, the term "1" is due to the quantum conductance, which can be ignored when $L \gg l_D$. Fig. 4(d) shows $LT_n(E_F)$ as a function of n, assuming $L \gg l_D (= 1\ \mu\text{m})$. G_n for both electrons and holes as a function of n is shown in Fig. 4(e).

The total conductance of a single GNR layer (in units of S) can be calculated as

$$G_{\text{total}} = \sum_n G_n(\text{electrons}) + \sum_n G_n(\text{holes}). \tag{4}$$

Equation (4) is valid for zz-GNRs. However, this is not valid for a practical narrow ac-GNR with $\Delta E_n = hv_f/2w > \max\{k_BT, |E_F|\}$, which can be assumed to be neither metallic nor semiconducting due to the inability of patterning ac-GNRs with the width accuracy of one atom. The valid expression of conductance for ac-GNR with $\Delta E_n > \max\{k_BT, |E_F|\}$ requires further investigation, but is not discussed in this paper. For both zz-GNRs and ac-GNRs, when $\Delta E_n \ll \max\{k_BT, |E_F|\}$, the summation can be transformed to an integration form as follows:

$$G_{\text{total}} \approx \frac{2}{\Delta E_n}\left[\int_0^{\infty} G_n(\text{electrons})dE_n + \int_{-\infty}^{0} G_n(\text{holes})dE_n\right] \tag{5}$$

which can further be derived as

$$G_{\text{total}} = \frac{1}{L}\frac{2q^2}{h} \cdot \frac{2w^2}{hv_f} \cdot 2k_BT \ln\left[2\cosh\left(\frac{E_F}{2k_BT}\right)\right] \cdot func(w, l_D) \tag{6a}$$

where

$$\begin{aligned} func(w, l_D) &= \begin{cases} \frac{\pi w - 2l_D}{l_D} + \frac{4\sqrt{l_D^2 - w^2}}{l_D} \cdot \operatorname{arctanh}\left(\sqrt{\frac{l_D - w}{l_D + w}}\right), & l_D \geq w \\ \frac{\pi w - 2l_D}{l_D} - \frac{4\sqrt{w^2 - l_D^2}}{l_D} \cdot \arctan\left(\sqrt{\frac{w - l_D}{w + l_D}}\right), & l_D < w \end{cases} \\ &\approx \begin{cases} 2\ln(l_D/w) + 2\ln 2 - 2 + \pi w/l_D, & l_D \gg w \\ \pi l_D/2w - 2l_D^2/3w^2, & l_D \ll w. \end{cases} \end{aligned} \tag{6b}$$

Note that the prefactor of 2 in (5) is from the degeneracy of $E_n = E_{-n}$. Detailed derivation of (6) is shown in Appendix.

The 2-D sheet conductance in siemens square can be derived from (6) as

$$\begin{aligned} G_{\text{sheet}} &= \lim_{w \to \infty} \frac{LG_{\text{total}}}{w} \\ &= \frac{2q^2}{h} \cdot \frac{\pi l_D}{hv_f} \cdot 2k_BT \ln\left[2\cosh\left(\frac{E_F}{2k_BT}\right)\right]. \end{aligned} \tag{7}$$

When $k_BT \ll |E_F|$, (7) reduces to [35, eq. (4)]

$$G_{\text{sheet}} = \frac{2q^2}{h} \cdot \frac{\pi l_D}{hv_f} \cdot |E_F| = \frac{q^2}{h} \cdot l_D \cdot k_F \tag{8}$$

where k_F is the wavenumber at the Fermi surface.

Fig. 5 shows the resistances of monolayer GNRs of different widths, if $l_D = 1\ \mu$m. It can be observed that the resistance difference between zz-GNRs and ac-GNRs is negligible

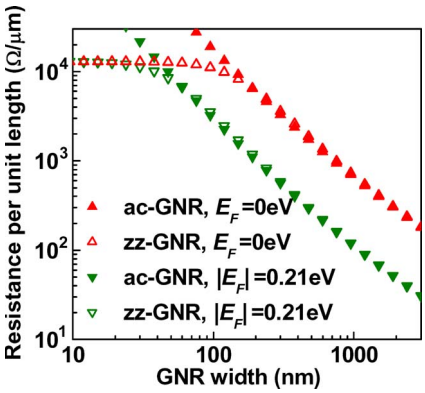

Fig. 5. Resistance of both neutral ($E_F = 0$ eV) and charged ($|E_F| = 0.21$ eV [3]) monolayer ac- and zz-GNRs, assuming $l_D = 1$ μm. zz-GNRs are assumed to have zero bandgap.

when GNR width is large enough, whereas the resistance of zz-GNRs is smaller than that of the corresponding ac-GNRs if $w < 45$ nm. However, as mentioned earlier, when the ac-GNR is narrow (which implies that ΔE_n becomes comparable with or greater than $\max\{k_B T, |E_F|\}$), the valid expression of conductance requires further investigation. For simplicity, the following analysis will only discuss zz-GNRs.

According to the above analysis, l_D plays an important role in determining the conductance. Theoretically, l_D of a monolayer GNR is proportional to its width (w) [26], [43], i.e.,

$$l_D(\text{GNR}) \approx \frac{2w}{\sqrt{3}} \cdot \frac{\gamma^2 - E^2/4}{\sigma_\varepsilon^2 + 4\sigma_\gamma^2} \approx \frac{4w}{\sqrt{3}} \cdot \frac{\gamma^2}{2\sigma_\varepsilon^2 + 8\sigma_\gamma^2} \quad (9)$$

where σ_ε and σ_γ are the variances of different Hamiltonian matrix elements [26], [46], E is the energy measured with respect to E_F, and $E \ll \gamma$. This is just like the MFP of CNTs as a function of their diameter (D) [46]–[48], i.e.,

$$l_D(\text{CNT}) = \pi D \cdot \sqrt{3}\gamma^2 / \left(2\sigma_\varepsilon^2 + 9\sigma_\gamma^2\right) \quad (10)$$

or

$$l_D(\text{CNT}) \approx 1000D. \quad (11)$$

Comparing (9)–(11), l_D of a monolayer GNR can be approximately expressed as

$$l_D(\text{GNR}) \approx 450w. \quad (12)$$

In reality, the experimental l_D value $(\sim 1$ μm) [20], [31] of monolayer GNRs is much smaller than that predicted by (12), as long as the width is not too small, which is due to the scattering from defects that is width independent. However, this is not a physical limit and can be improved as fabrication technology progresses. In the following analysis, an optimistic but arbitrary value of $l_D = 5$ μm (which is $\leq 450w$ but $>$ 1 μm) is assumed for monolayer GNRs. It will be shown that even with this optimistic MFP, monolayer GNRs cannot match the performance of Cu interconnects.

In multilayer GNRs, the MFP and conductance per layer is reduced because of intersheet electron hopping [35], which is insensitive to width. The MFP of multilayer GNRs can be

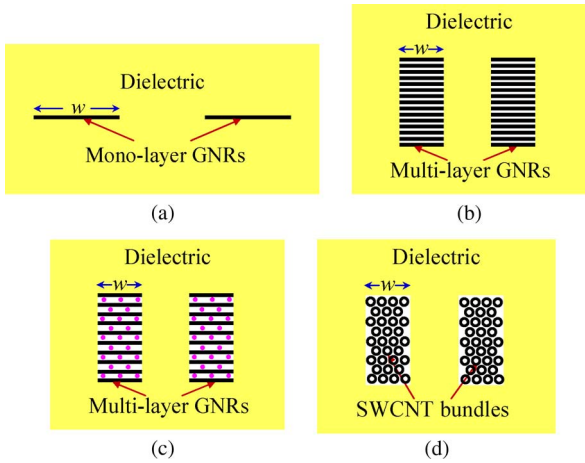

Fig. 6. Schematic view of (a) monolayer GNRs, (b) neutral multilayer GNRs (graphite), (c) intercalation-doped multilayer GNRs (graphite), and (d) SWCNT bundles for interconnect applications.

extracted from experimental results of bulk graphite (details of the extraction are shown in Section III). It should be noted that there is a report that the adjacent layers do not interact with each other in multilayer GNRs grown on C-faced 4H-SiC $(000\bar{1})$ [32], [49]. However, this type of multilayer GNRs is an unlikely candidate for interconnect applications due to two reasons: 1) Interconnect wires are fabricated on top of dielectrics, but not single-crystal SiC, and 2) adjacent layers are rotated by $30^\circ \pm 2.204^\circ$, which implies that if the first GNR layer is zigzag edge, the second layer becomes approximately armchair edge, and there is no report of how to perform intercalation doping (discussed in Section III) in such GNRs, which would imply low conductance.

III. Resistance Comparison of GNRs With Other Materials

Fig. 6 shows different structures of GNRs and the structure of SWCNT bundles that are simulated for possible interconnect applications. The MFP of neutral multilayer GNR (graphite) is extracted as 419 nm from the in-plane conductivity of 0.026 $(\mu\Omega \cdot \text{cm})^{-1}$ [35] and layer spacing of 0.34 nm by setting $E_F = 0$ and solving (7). Note that the number of GNR layers is equal to the total height divided by the layer spacing. For example, a multilayer GNR with a height of 22 nm has 65 layers. The in-plane conductivity of graphite can be increased by several tens of magnitude by intercalation doping (or exohedral doping), which involves an insertion of one dopant layer between each pair of adjacent graphene layers. The level of intercalation doping can be indicated by stage indexes: stage g indicates that there are g graphene layers between each pair of adjacent intercalation layers (Fig. 7). The value of g can be controlled by process conditions such as the intercalant vapor pressure [41]. Intercalation doping can increase the carrier density due to charge transfer and can increase the MFP due to increased layer spacing (interlayer scattering is suppressed) [40]. For example, the stage-2 AsF_5 intercalated graphite (p-type) can have in-plane conductivity of 0.63 $(\mu\Omega \cdot \text{cm})^{-1}$, which is slightly greater than the bulk conductivity of Cu, with a hole volume concentration (n_p) of 4.6×10^{20} cm^{-3}

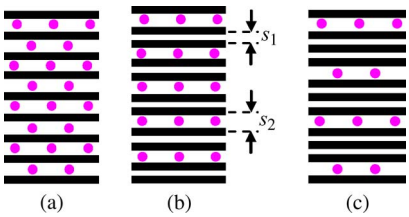

Fig. 7. Schematic view of (a) stage-1, (b) stage-2, and (c) stage-3 intercalation-doped multilayer GNRs (graphite). The solid lines indicate graphene layers, while the dots indicate intercalation dopant layers. s_1 and s_2 are the layer spacing between two adjacent graphene layers. In stage-2 AsF_5 intercalated graphite, $s_1 = 0.335$ nm and $s_2 = 0.815$ nm [41].

[50]. The average layer spacing $(s = (s_1 + s_2)/2)$ between two adjacent graphene layers is 0.575 nm for stage-2 intercalated graphite, according to Fig. 7(b). Using the simplified tight-binding model, the relationship between E_F and hole density per layer $(n_{p0} = n_p s)$ is expressed as

$$n_{p0} = 4\pi(k_F/2\pi)^2 = 4\pi(E_F/hv_f)^2. \tag{13}$$

For such type of intercalation-doped graphite, $|E_F| = 0.60$ eV is obtained from (13), and $l_D = 1.03$ μm is obtained from (7). It should be noted that intercalated graphite with even larger conductivity $(\sim 1(\mu\Omega \cdot \text{cm})^{-1})$ has been reported in [42], however, this is not used in this work because of lack of data (l_D and E_F cannot be obtained if carrier concentration is not known). It should also be noted that using the band structure of graphene is a good approximation for the analysis of AsF_5-doped graphite due to the following two reasons: 1) interlayer interaction of AsF_5-doped graphite is suppressed as compared to neutral graphite (with band overlap of 0.04 eV between conduction and valence bands) and 2) $E_F = -0.60$ eV, which is far outside the band overlap region. For the undoped (neutral) graphite, the overlap of 0.04 eV is in the same order of k_BT. This may induce some errors in the estimation of conductance but does not change the result qualitatively.

In addition to the GNRs, Cu, SWCNT bundles, and W are also discussed in this section for comparison. The geometry of the wires and the resistivity for Cu wire are obtained from the ITRS [44]. The resistance model for SWCNT bundles is derived in [48]: when one-third of the SWCNTs are metallic, the conductivity can be expressed as

$$\sigma(\text{SWCNT bundles}) \approx \frac{1}{3}\frac{4q^2 l_D/h}{(D+s)^2\sqrt{3}/2} \tag{14}$$

where s is minimum spacing between adjacent SWCNTs, and D is the diameter of SWCNTs. When $s = 0.34$ nm, $D = 1$ nm and $l_D = 1$ μm [48], $\sigma(\text{SWCNT bundles}) = 0.33\ (\mu\Omega \cdot \text{cm})^{-1}$. The resistivity model for W wire is adapted from [51] and [52], which is described by

$$\rho = \rho_0 \left\{ \frac{1}{3} \Big/ \left[\frac{1}{3} - \frac{\alpha}{2} + \alpha^2 - \alpha^3 \ln\left(1 + \frac{1}{\alpha}\right) \right] + \frac{3}{8} C(1-p) \frac{1+AR}{AR} \frac{l_D}{w} \right\} \tag{15}$$

where

$$\alpha = (l_D/d)R/(1-R) \tag{16}$$

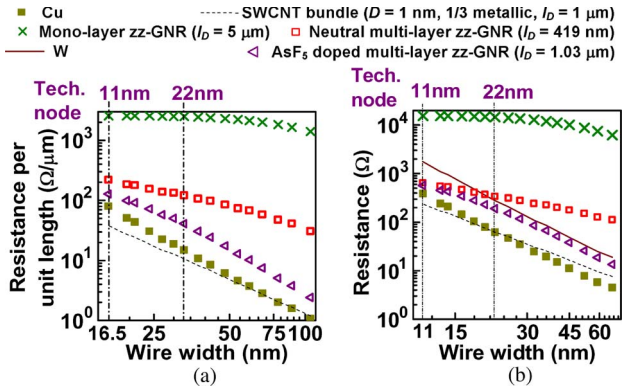

Fig. 8. Resistance comparison of (a) long global wires and (b) $L = 1$ μm local wires among Cu, W, SWCNT bundles, and different types of GNRs. For monolayer GNRs, $l_D = 5$ μm and $|E_F| = 0.21$ eV; for neutral multilayer GNRs, $l_D = 419$ nm (fixed); for stage-2 AsF_5-doped multilayer GNRs, average layer spacing is 0.575 nm, fixed $l_D = 1.03\mu$m, and $|E_F| = 0.60$ eV. Specularity (p) is assumed to be zero; zz-GNRs are assumed to have zero bandgap. Note that W is not considered for global wires due to its high resistivity.

$\rho_0 = 8.7$ $\mu\Omega \cdot$ cm is the resistivity of the bulk material, AR is the aspect ratio, w is the wire width, $l_D = 33$ nm is the MFP, $d = w/2$ is the average distance between grain boundaries, $p = 0.3$ is the specularity parameter, $R = 0.25$ is the reflectivity coefficient at grain boundaries, and $C = 1.2$ is an empirical parameter.

The wire resistances of different types of both global and local interconnects are compared in Fig. 8. Beyond the 22-nm technology node, SWCNT bundles are the best, while all of the GNR structures are not better than Cu—for both global and local wires. However, an AsF_5-doped multilayer GNR is always better than W.

A zero bandgap of zz-GNRs is assumed in the above analysis. However, in reality, a bandgap is induced because of the staggered sublattice potential from magnetic ordering once electron spin is considered [37], [38]. The bandgap of zz-GNRs increases with decreasing wire width [the bandgap, in electronvolts, is $0.933/(w + 1.5)$, with w in nanometers]. In such a situation, (2) can be modified as

$$E_0 = \frac{0.933}{2(w+1.5)} \qquad |E_n| = \left(|n| + \frac{1}{2}\right) \cdot \frac{hv_f}{2w} \qquad \text{for } n \neq 0. \tag{17}$$

If (26) in Appendix and (3) are still assumed to be valid for zeroth conduction modes, the total conductance should then be calculated directly from (4). The calculated results for both monolayer and multilayer GNRs are shown in Fig. 9. It is shown that the resistance of narrow width zz-GNRs becomes even worse after such consideration, particularly for the monolayer GNRs and neutral multilayer GNRs. This resistance change is primarily because of the edge scattering in the zeroth conduction mode, which is not an issue if E_0 is assumed to be zero.

Fig. 10 shows the conductance contour plots as a function of both l_D and E_F for both bulk graphite and 16.5-nm-wide (minimum global wire width for the 11-nm technology node) multilayer zz-GNRs. In the contour plots, the slopes of the

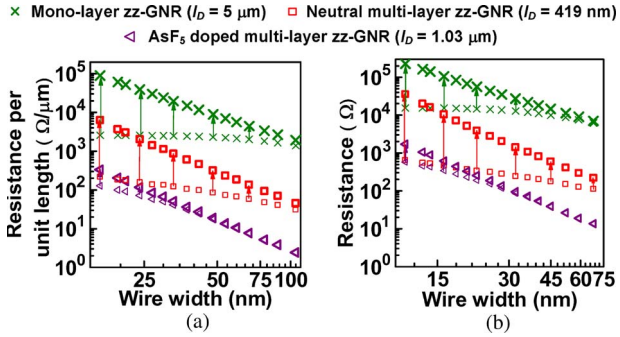

Fig. 9. Impact of the bandgap of zz-GNRs on resistance estimation of (a) long global wires and (b) $L = 1$ μm local wires. l_D, $|E_F|$, specularity, and average layer spacing in monolayer GNRs and neutral and stage-2 AsF_5-doped multilayer GNRs are the same as in Fig. 8. The arrows indicate the resistance changes after consideration of the bandgap of zz-GNRs (smaller and bigger symbols indicate before and after such consideration, respectively).

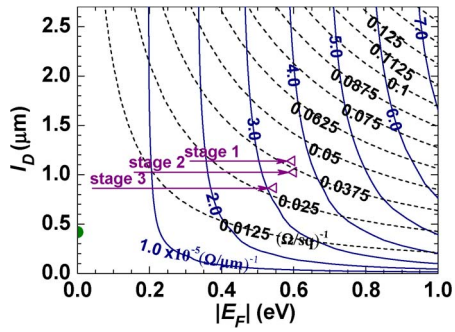

Fig. 10. Conductance contours as a function of Fermi level $|E_F|$ and MFP l_D. Solid lines show the conductance per layer of 16.5-nm-wide (minimum global wire width in the 11-nm technology node) long global multilayer zz-GNR wires. Dashed lines show the sheet conductance per layer of bulk graphite. The "dot" on the lower left-hand side represents neutral graphite, while the "open triangles" represent the three stages of AsF_5 intercalation-doped graphite [50]. p is assumed to be 0. The bandgap of zz-GNRs and the edge scattering of the zeroth conduction mode are considered.

contour lines, $(\partial l_D/\partial|E_F|)_G$, indicate the importance of the two parameters, i.e., l_D and E_F. We have

$$\frac{|E_F|}{G}\left(\frac{\partial G}{\partial|E_F|}\right)_{l_D}\Big/\frac{l_D}{G}\left(\frac{\partial G}{\partial l_D}\right)_{E_F}=-\frac{|E_F|}{l_D}\left(\frac{\partial l_D}{\partial|E_F|}\right)_G \tag{18}$$

where G is either the conductance per layer of $w = 16.5$ nm multilayer zz-GNRs or the sheet conductance per layer of graphite, and $(\partial z/\partial x)_y$ stands for the partial differential of z to x when maintaining a fixed y for three correlated variables x, y, and z. Therefore, steeper contour lines indicate higher importance of E_F. Hence, the plots indicate that l_D and E_F are equally important for bulk graphite ($|E_F|/l_D \cdot (\partial l_D/\partial|E_F|)_G = -1$), but E_F is more important if $l_D \gg w$ for very narrow zz-GNRs (contour lines are steeper). Note that this statement is contrary to that in [43], which is due to the consideration of the bandgap of zz-GNRs and the edge scattering of zeroth conduction mode in this paper: the edge scattering of zeroth conduction mode, which is independent of l_D [refer to the third term in (3)], becomes the dominant factor in determining the conductance.

Complete diffusive edges are assumed in the above analysis, but the GNR conductance can be improved by improving the

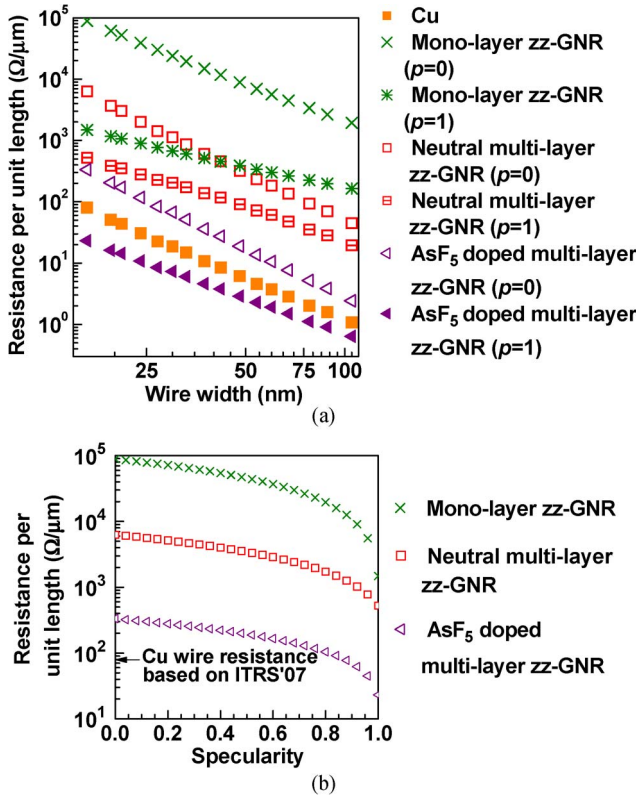

Fig. 11. Impact of edge specularity of multilayer zz-GNRs on long global wire's resistance: (a) resistance versus width and (b) resistance versus specularity ($w = 16.5$ nm and $AR = 2.9$). l_D, $|E_F|$, and average layer spacing in monolayer GNRs and neutral and stage-2 AsF_5-doped multilayer GNRs are the same as in Fig. 8. The bandgap of zz-GNRs and the edge scattering of the zeroth conduction mode are considered.

specularity (p) of the edges. Recently, a backscattering probability of 0.2 [53], or equivalently, $p = 0.8$, has been achieved. The specularity effect can be modeled by multiplying the term $L/w\cot\theta$ (term of edge scattering) in (3) by $(1-p)$, i.e.,

$$\frac{1}{T_n(E)}=1+\frac{L}{l_D\cos\theta}+\frac{L(1-p)}{w\cot\theta}\approx\frac{L}{l_D\cos\theta}+\frac{L(1-p)}{w\cot\theta}. \tag{19}$$

It can be observed in Fig. 11 that the conductance of zz-GNR can be improved significantly if the edges change from completely diffusive $(p = 0)$ to completely specular $(p = 1)$. However, even for $p = 1$, monolayer and neutral multilayer GNRs are not better than Cu. Furthermore, only if p is very close to 1 can the AsF_5-doped multilayer zz-GNRs be better than Cu.

For local interconnects, where wire length can be comparable to or smaller than l_D, the quantum contact resistance cannot be ignored. Similar to CNTs, the quantum contact resistance for GNRs is $h/2q^2$ for each conduction mode. The per unit length wire resistances as a function of length of different structures are shown in Fig. 12. It should be noted that the quantum contact resistance is the lower limit of contact resistance in CNT/GNR interconnects. In reality, the situation could even be worse because of the imperfect contact resistance, which is fabrication technology dependent.

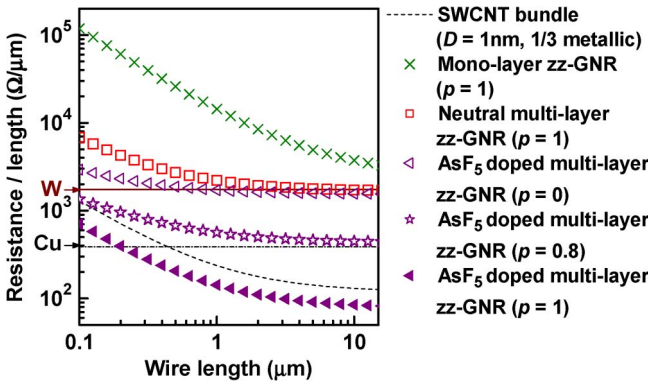

Fig. 12. Impact of quantum contact resistance on local wire resistance ($w =$ 11 nm and $AR = 2.1$). l_D, $|E_F|$, and average layer spacing in monolayer GNRs and neutral and stage-2 AsF_5-doped multilayer GNRs are the same as in Fig. 8. The bandgap of zz-GNRs and the edge scattering of the zeroth conduction mode are considered.

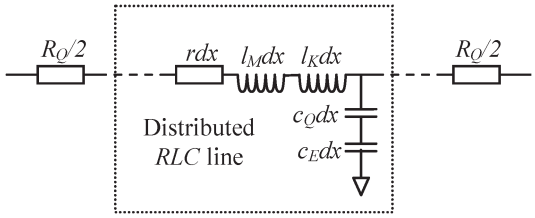

Fig. 13. RLC model of GNR interconnects (assuming perfect contact).

IV. RLC Delay Model for GNR Interconnects

In addition to the resistance, the capacitance and inductance are also important to the propagation delay. Similar to the CNTs [8], the distributed capacitance of GNRs contains both the electrostatic and quantum capacitances, while the distributed inductance contains both the magnetic and kinetic inductances. The distributed RLC equivalent circuit for GNRs is shown in Fig. 13. R_Q is the quantum contact resistance defined as

$$R_Q = (h/2q^2)/N_{\rm ch}N_{\rm layer} \tag{20}$$

where $N_{\rm ch}$ is the number of conducting channels (modes) in one layer, $N_{\rm layer}$ is the number of GNR layers, $r = r_{\rm one\ layer}/N_{\rm layer}$ is the distributed scattering resistance, c_Q and c_E are the quantum and electrostatic capacitance, respectively, and l_K and l_M are the kinetic and magnetic inductance, respectively. c_Q can be expressed as

$$c_Q = N_{\rm layer}N_{\rm ch}4q^2/hv_f. \tag{21}$$

l_K can be expressed as

$$l_K = (h/4q^2v_f)/N_{\rm layer}N_{\rm ch} \tag{22}$$

where v_f is the Fermi velocity. and $N_{\rm ch}$ can be expressed as

$$\begin{aligned} N_{\rm ch} &= N_{\rm ch,electron} + N_{\rm ch,hole} \\ &= \sum_n \left[1 + \exp\left(\frac{E_{n,\rm electron} - E_F}{k_BT}\right)\right]^{-1} \\ &\quad + \sum_n \left[1 + \exp\left(\frac{E_F - E_{n,\rm hole}}{k_BT}\right)\right]^{-1} \end{aligned} \tag{23}$$

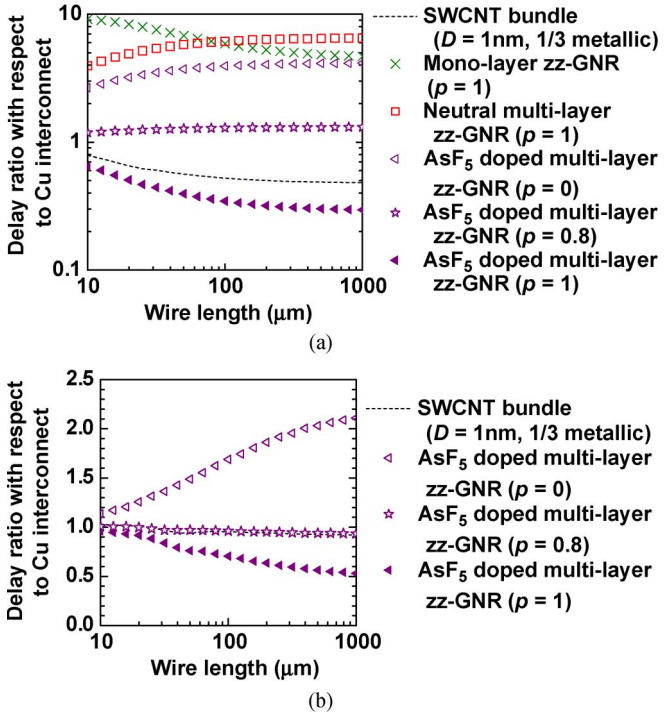

Fig. 14. RLC delay ratio (at the 11-nm technology node) with respect to Cu wire for global interconnects (height is 2.9 × 16.5 nm), with a wire width of (a) minimum value = 16.5 nm and (b) 82.5 nm (curves for monolayer and neutral multilayer zz-GNRs are out of range); 50 times minimum driver size and load. l_D, $|E_F|$, and average layer spacing in monolayer GNRs and neutral and stage-2 AsF_5-doped multilayer GNRs are the same as in Fig. 8. The bandgap of zz-GNRs and the edge scattering of the zeroth conduction mode are considered.

where $E_{n,\rm electron}$ ($E_{n,\rm hole}$) is the minimum (maximum) energy of the nth conduction (valence) subband. Generally, the kinetic inductance in monolayer GNRs is much larger than the magnetic inductance, while that is not always the case in multilayer GNRs. On the other hand, the quantum capacitance in multilayer GNRs is much larger than the electrostatic capacitance, while that is not always the case in monolayer GNRs.

V. Performance Comparison of GNRs With Other Materials

The delay of both global and local interconnects in the 11-nm technology node are analyzed based on the distributed RLC model in Fig. 13. The quantum capacitances and kinetic inductances are obtained from (21) and (22), while electrostatic capacitances and magnetic inductances are obtained from the predictive technology model [54]. Simulations were implemented using HSPICE. The driver equivalent resistance and capacitance are obtained from the 11-nm technology node (ITRS 2007) [44].

Fig. 14 shows the comparison with respect to Cu global interconnects. The performance of monolayer zz-GNR and neutral multilayer zz-GNR is much worse than Cu, even if a complete specular edge is assumed. The multilayer zz-GNR can match or become better than Cu only if it is intercalation (AsF_5) doped and if it has very specular edges ($p > 0.8$). The AsF_5-doped multilayer zz-GNRs can even be better than SWCNT bundles if $p = 1$ is achieved. However, for more

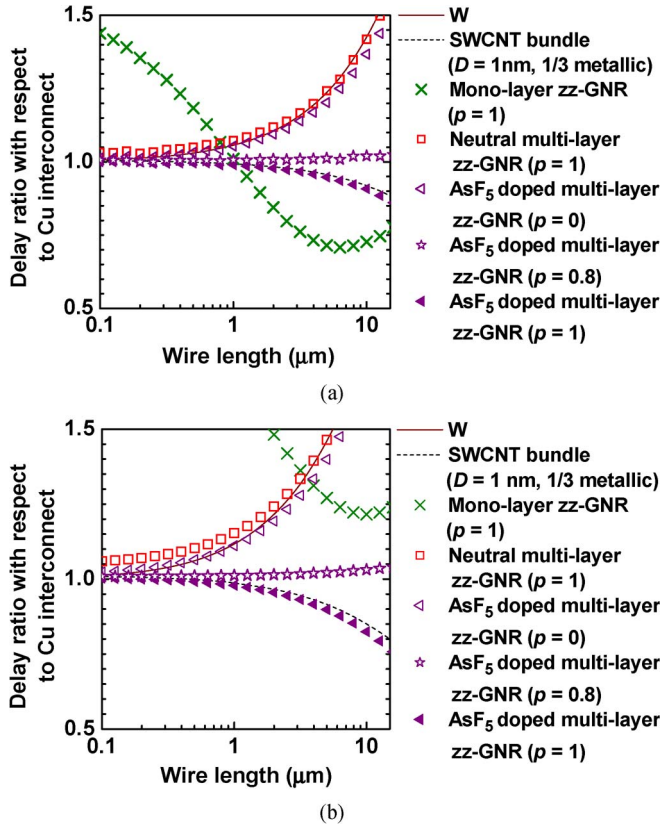

Fig. 15. RLC fanout-of-4 delay ratio with respect to Cu wire (local interconnect, $w = 11$ nm, $AR = 2.1$), with (a) minimum driver size and (b) double the minimum driver size. l_D, $|E_F|$, and average layer spacing in monolayer GNRs and neutral and stage-2 AsF_5-doped multilayer GNRs are the same as in Fig. 8. The bandgap of zz-GNRs and the edge scattering of the zeroth conduction mode are considered.

practical edge specularity, i.e., $p = 0.2-0.6$, GNRs cannot match the performance of Cu or that of SWCNT bundles (even for metallic fraction = 1/3) at the global level, until the very end of the ITRS (11-nm technology node). It is worth noting that for global interconnects, MWCNT bundles are better than SWCNT bundles (for metallic fraction = 1/3) [48], which implies that GNRs cannot match the performance of MWCNT bundles.

For local interconnects (Fig. 15), the performance of AsF_5-doped multilayer zz-GNRs can either match or be better than that of Cu, only if it has very specular edges ($p > 0.8$). The AsF_5-doped multilayer zz-GNRs can be slightly better than SWCNT bundles if $p = 1$ is achieved. The monolayer zz-GNRs are worse than Cu for most cases, even if complete specular edge is achieved, although it can be better than Cu in some special cases (minimum driver size and several micrometer wire lengths) due to their smaller capacitance. The neutral multilayer GNRs are not even better than W, even if complete specular edge is achieved. However, the AsF_5-doped multilayer zz-GNRs are better than W in most cases, which suggest possible application of zz-GNRs as local interconnects.

The overall results are summarized in Table II. In general, until the very end of the roadmap (11-nm technology node), GNRs are not better than Cu, unless some special technology improvements are achieved: multilayer zz-GNR with proper intercalation doping and very specular edges.

TABLE II
PERFORMANCE COMPARISON OF DIFFERENT MATERIALS WITH RESPECT TO Cu AT THE 11-nm TECHNOLOGY NODE OF ITRS 2007

Interconnect Material	Global	Local
Tungsten (W)	-	worse
SWCNT (D=1nm, 1/3 metallic)	better	better
MWCNT	much better [48]	worse [48]
Mono-layer GNR (p=1)	much worse	worse for most cases
Neutral multi-layer GNR (p=1)	much worse	worse
AsF_5 doped multi-layer GNR (p=0)	worse	worse
AsF_5 doped multi-layer GNR (p=0.8)	comparable	comparable
AsF_5 doped multi-layer GNR (p=1)	much better	better

VI. CONCLUSION

In this paper, GNRs have been analyzed from fundamental physics to their industrial prospects as VLSI interconnects. Monolayer, neutral multilayer, and intercalation-doped multilayer zz-GNR interconnects are analyzed from both conductance and propagation delay perspectives. The conductance of GNRs, which were analytically derived using a simple tight-binding method and the Landauer formalism, accounted for edge scattering of the zeroth conduction modes and small bandgap in narrow zz-GNRs. A comparative analysis (with other interconnect materials: Cu, CNTs, and W) was carried out for interconnect geometries until the very end of ITRS 2007 (11-nm technology node). The analysis reveals that although GNRs appear to have some fabrication advantages over CNTs (for horizontal interconnects) in order for them to match (or better) the performance of Cu or that of CNT bundles at both the global and local levels, some special technology improvements must be achieved. More specifically, it is shown that proper intercalation doping and very specular edges ($p > 0.8$) are necessary to make multilayer zz-GNR interconnects comparable to or better than Cu or CNT interconnects at either the global or local level. On the other hand, intercalation-doped multilayer zz-GNRs at the local level can have better performance than that of tungsten (even for $p = 0$), implying possible application as local interconnects in some cases.

APPENDIX

Equation (6) can be derived from (5) as follows:

$$\begin{aligned}\int_0^\infty G_n(\text{electrons})dE_n &= \int_0^\infty \frac{2q^2}{h}dE_n \int_{E_n}^\infty T_n(E)\left(-\frac{\partial f_0}{\partial E}\right)dE \\ &= \frac{2q^2}{h}\int_0^\infty \left(-\frac{\partial f_0}{\partial E}\right)dE \int_0^E T_n(E)dE_n \\ &= \frac{2q^2}{h}\int_0^\infty E\left(-\frac{\partial f_0}{\partial E}\right)dE \int_0^E \frac{1}{E}T_n(E)dE_n\end{aligned} \tag{24}$$

where

$$|E_n| = \hbar v_f |k_y| \quad |E| = \hbar v_f \sqrt{k_x^2 + k_y^2} \tag{25}$$

where k_x and k_y are the wave vector components along and across the GNR, respectively, and

$$|\tan\theta| = |k_y/k_x| \quad |\sin\theta| = |E_n/E|. \tag{26}$$

Therefore, one of the integrals in (24) can be evaluated as

$$\int_0^E \frac{1}{E} T_n(E) dE_n \approx \int_0^{\pi/2} \frac{1}{L} \left(\frac{1}{l_D \cos\theta} + \frac{1}{w \cot\theta} \right)^{-1} \cos\theta \, d\theta = \frac{1}{2L} w \cdot func(w, l_D) \tag{27}$$

where $func(w, l_D)$ is given in (6b), i.e.,

$$func(w, l_D) = \begin{cases} \frac{\pi w - 2l_D}{l_D} + \frac{4\sqrt{l_D^2 - w^2}}{l_D} \cdot \operatorname{arctanh}\left(\sqrt{\frac{l_D - w}{l_D + w}} \right), & l_D \geq w \\ \frac{\pi w - 2l_D}{l_D} - \frac{4\sqrt{w^2 - l_D^2}}{l_D} \cdot \arctan\left(\sqrt{\frac{w - l_D}{w + l_D}} \right), & l_D < w \end{cases} \approx \begin{cases} 2\ln(l_D/w) + 2\ln 2 - 2 + \pi w/l_D, & l_D \gg w \\ \pi l_D/2w - 2l_D^2/3w^2, & l_D \ll w. \end{cases}$$

Note that the integration is from 0 to $\pi/2$ rather than $-\pi/2$ to $\pi/2$ because the degeneracy prefactor of $E_n = E_{-n}$ is already included in (5). The other integral in (24) can be evaluated as

$$\int_0^\infty E\left(-\frac{\partial f_0}{\partial E} \right) dE = \int_0^\infty -E \frac{\partial}{\partial E} \left(\frac{1}{1 + \exp\left[(E - E_F)/k_B T \right]} \right) dE = \int_0^\infty \frac{E}{4k_B T \cosh^2\left(\frac{E - E_F}{2k_B T} \right)} dE = k_B T \ln\left[1 + \exp\left(\frac{E_F}{k_B T} \right) \right]. \tag{28}$$

Therefore,

$$\int_0^\infty G_n(\text{electrons}) dE_n = (2q^2/h) \cdot k_B T \ln \times \left[1 + \exp(E_F/k_B T) \right] \cdot \frac{1}{2L} w \cdot func(w, l_D). \tag{29}$$

Similarly

$$\int_{-\infty}^0 G_n(\text{holes}) dE_n = (2q^2/h) \cdot k_B T \ln \times \left[1 + \exp(-E_F/k_B T) \right] \cdot \frac{1}{2L} w \cdot func(w, l_D). \tag{30}$$

From (5) and if $\Delta E_n = h v_f / 2w$, we get

$$G_{\text{total}} \approx \frac{2}{\Delta E_n} \left[\int_0^\infty G_n(\text{electrons}) dE_n + \int_{-\infty}^0 G_n(\text{holes}) dE_n \right] = \frac{1}{L} \frac{2q^2}{h} \cdot \frac{2w^2}{h v_f} \cdot 2k_B T \ln\left[2\cosh\left(\frac{E_F}{2k_B T} \right) \right] \cdot func(w, l_D) \tag{31}$$

which is the same as (6).

REFERENCES

[1] M. C. Lemme, T. J. Echtermeyer, M. Baus, and H. Kurz, "A graphene field-effect device," *IEEE Electron Device Lett.*, vol. 28, no. 4, pp. 282–284, Apr. 2007.

[2] Q. Shao, G. Liu, D. Teweldebrhan, and A. A. Balandin, "High-temperature quenching of electrical resistance in graphene interconnects," *Appl. Phys. Lett.*, vol. 92, no. 20, p. 202 108, May 2008.

[3] A. Naeemi and J. D. Meindl, "Conductance modeling for graphene nanoribbon (GNR) interconnects," *IEEE Electron Device Lett.*, vol. 28, no. 5, pp. 428–431, May 2007.

[4] A. Naeemi and J. D. Meindl, "Performance benchmarking for graphene nanoribbon, carbon nanotube, and Cu interconnects," in *Proc. IEEE Int. Interconnect Technol. Conf.*, San Francisco, CA, 2008, pp. 183–185.

[5] A. K. Geim and K. S. Novoselov, "The rise of graphene," *Nat. Mater.*, vol. 6, no. 3, pp. 183–191, Mar. 2007.

[6] F. Kreupl, A. P. Graham, M. Liebau, G. S. Duesberg, R. Seidel, and E. Unger, "Carbon nanotubes for interconnect applications," in *IEDM Tech. Dig.*, Dec. 2004, pp. 683–686.

[7] N. Srivastava and K. Banerjee, "Interconnect challenges for nanoscale electronic circuits," *TMS J. Mater.*, vol. 56, no. 10, pp. 30–31, Oct. 2004.

[8] N. Srivastava, H. Li, F. Kreupl, and K. Banerjee, "On the applicability of single-walled carbon nanotubes as VLSI interconnects," *IEEE Trans. Nanotechnol.*, vol. 8, no. 7, 2009.

[9] M. Radosavljević, J. Lefebvre, and A. T. Johnson, "High-field electrical transport and breakdown in bundles of single-wall carbon nanotubes," *Phys. Rev. B, Condens. Matter*, vol. 64, no. 24, p. 241 307, Dec. 2001.

[10] B. Q. Wei, R. Vajtai, and P. M. Ajayan, "Reliability and current carrying capacity of carbon nanotubes," *Appl. Phys. Lett.*, vol. 79, no. 8, pp. 1172–1174, Aug. 2001.

[11] K. S. Novoselov, A. K. Geim, S. V. Morozov, D. Jiang, Y. Zhang, S. V. Dubonos, I. V. Grigorieva, and A. A. Firsov, "Electric field effect in atomically thin carbon films," *Science*, vol. 306, no. 5696, pp. 666–669, Oct. 2004.

[12] F. Li, H. M. Cheng, S. Bai, G. Su, and M. S. Dresselhaus, "Tensile strength of single-walled carbon nanotubes directly measured from their macroscopic ropes," *Appl. Phys. Lett.*, vol. 77, no. 20, pp. 3161–3163, Nov. 2000.

[13] M.-F. Yu, O. Lourie, M. J. Dyer, K. Moloni, T. F. Kelly, and R. S. Ruoff, "Strength and breaking mechanism of multiwalled carbon nanotubes under tensile load," *Science*, vol. 287, no. 5453, pp. 637–640, Jan. 2000.

[14] J. Hone, M. Whitney, C. Piskoti, and A. Zettl, "Thermal conductivity of single-walled carbon nanotubes," *Phys. Rev. B, Condens. Matter*, vol. 59, no. 4, pp. R2 514–R2 516, Jan. 1999.

[15] P. Kim, L. Shi, A. Majumdar, and P. L. McEuen, "Thermal transport measurements of individual multiwalled carbon nanotubes," *Phys. Rev. Lett.*, vol. 87, no. 21, p. 215 502, Oct. 2001.

[16] A. A. Balandin, S. Ghosh, W. Bao, I. Calizo, D. Teweldebrhan, F. Miao, and C. N. Lau, "Superior thermal conductivity of single-layer graphene," *Nano Lett.*, vol. 8, no. 3, pp. 902–907, Mar. 2008.

[17] S. Ghosh, I. Calizo, D. Teweldebrhan, E. P. Pokatilov, D. L. Nika, A. A. Balandin, W. Bao, F. Miao, and C. N. Lau, "Extremely high thermal conductivity of graphene: Prospects for thermal management applications in nanoelectronic circuits," *Appl. Phys. Lett.*, vol. 92, no. 15, p. 151 911, Apr. 2008.

[18] P. L. McEuen, M. S. Fuhrer, and H. Park, "Single-walled carbon nanotube electronics," *IEEE Trans. Nanotechnol.*, vol. 1, no. 1, pp. 78–85, Mar. 2002.

[19] H. J. Li, W. G. Lu, J. J. Li, X. D. Bai, and C. Z. Gu, "Multichannel ballistic transport in multiwall carbon nanotubes," *Phys. Rev. Lett.*, vol. 95, no. 8, p. 086 601, Aug. 2005.

[20] K. I. Bolotin, K. J. Sikes, J. Hone, H. L. Stormer, and P. Kim, "Temperature dependent transport in suspended graphene," *Phys. Rev. Lett.*, vol. 101, no. 9, p. 096 802, Aug. 2008.

[21] Y. Awano, "Carbon nanotube technologies for LSI via interconnects," *IEICE Trans. Electron.*, vol. E89-C, no. 11, pp. 1499–1503, Nov. 2006.

[22] Q. Yu, J. Lian, S. Siriponglert, H. Li, Y. P. Chen, and S.-S. Pei, "Graphene segregated on Ni surfaces and transferred to insulators," *Appl. Phys. Lett.*, vol. 93, no. 11, p. 113 103, Nov. 2008.

[23] D. N. Futaba, K. Hata, T. Yamada, T. Hiraoka, Y. Hayamizu, Y. Kakudate, O. Tanaike, H. Hatori, M. Yumura, and S. Iijima, "Shape-engineerable and highly densely packed single-walled carbon nanotubes and their application as super-capacitor electrodes," *Nat. Mater.*, vol. 5, no. 12, pp. 987–994, Dec. 2006.

[24] P. R. Wallace, "The band theory of graphite," *Phys. Rev.*, vol. 71, no. 9, pp. 622–634, May 1947.

[25] M. Dresselhaus, *The Novel Nanostructures of Carbon*, Jan. 2008. University of Tokyo Lecture. [Online]. Available: www.photon.t.u-tokyo.ac.jp/~maruyama/visitors/DresselhausPres.pdf
[26] D. A. Areshkin, D. Gunlycke, and C. T. White, "Ballistic transport in graphene nanostrips in the presence of disorder: Importance of edge effects," *Nano Lett.*, vol. 7, no. 1, pp. 204–210, Jan. 2007.
[27] K. Nakada, M. Fujita, G. Dresselhaus, and M. S. Dresselhaus, "Edge state in graphene ribbons: Nanometer size effect and edge shape dependence," *Phys. Rev. B, Condens. Matter*, vol. 54, no. 24, pp. 17 954–17 961, Dec. 1996.
[28] L. Malysheva and A. Onipko, *Dispersion of 'Dispersionless Band': Comments on L. Brey and H. A. Fertig Paper Electronic States of Graphene Nanoribbons Studied With the Dirac Equation*, May 2008. arXiv:0802.1385v2 [cond-mat.mes-hall].
[29] P. Shemella and S. K. Nayak, "Electronic structure and band-gap modulation of graphene via substrate surface chemistry," *Appl. Phys. Lett.*, vol. 94, no. 3, p. 032 101, Jan. 2009.
[30] G. Aichmayr, A. Avellán, G. S. Duesberg, F. Kreupl, S. Kudelka, M. Liebau, A. Orth, A. Sänger, J. Schumann, and O. Storbeck, "Carbon/high-k trench capacitor for the 40 nm DRAM generation," in *VLSI Symp. Tech. Dig.*, Jun. 2007, pp. 186–187.
[31] C. Berger, Z. Song, X. Li, X. Wu, N. Brown, C. Naud, D. Mayou, T. Li, J. Hass, A. N. Marchenkov, E. H. Conrad, P. N. First, and W. A. de Heer, "Electronic confinement and coherence in patterned epitaxial graphene," *Science*, vol. 312, no. 5777, pp. 1191–1196, Apr. 2006.
[32] J. Hass, R. Feng, T. Li, X. Li, Z. Zong, W. A. de Heer, P. N. First, E. H. Conrada, C. A. Jeffrey, and C. Berger, "Highly ordered graphene for two dimensional electronics," *Appl. Phys. Lett.*, vol. 89, no. 14, p. 143 106, Oct. 2006.
[33] J. C. Meyer, A. K. Geim, M. I. Katsnelson, K. S. Novoselov, T. J. Booth, and S. Roth, "The structure of suspended graphene sheets," *Nature*, vol. 446, no. 7131, pp. 60–63, Mar. 2007.
[34] X. Li, W. Cai, J. An, S. Kim, J. Nah, D. Yang, R. Piner, A. Velamakanni, I. Jung, E. Tutuc, S. K. Banerjee, L. Colombo, and R. S. Ruoff, "Large-area synthesis of high-quality and uniform graphene films on copper foils," *Science Express Reports*, vol. 324, no. 5932, pp. 1312–1314, Jun. 2009.
[35] L. X. Benedict, V. H. Crespi, S. G. Louie, and M. L. Cohen, "Static conductivity and superconductivity of carbon nanotubes—Relations between tubes and sheets," *Phys. Rev. B, Condens. Matter*, vol. 52, no. 20, pp. 14 935–14 940, Nov. 1995.
[36] B. Partoens and F. M. Peeters, "From graphene to graphite: Electronic structure around the K point," *Phys. Rev. B, Condens. Matter*, vol. 74, no. 7, p. 075 404, Aug. 2006.
[37] Y.-W. Son, M. L. Cohen, and S. G. Louie, "Energy gaps in graphene nanoribbons," *Phys. Rev. Lett.*, vol. 97, no. 21, p. 216 803, Nov. 2006.
[38] X. Li, X. Wang, L. Zhang, S. Lee, and H. Dai, "Chemically derived, ultra smooth graphene nanoribbon semiconductors," *Science*, vol. 319, no. 5867, pp. 1229–1232, Feb. 2008.
[39] L. Ci, Z. Xu, L. Wang, W. Gao, F. Ding, K. Kelly, B. Yakobson, and P. Ajayan, "Controlled nanocutting of graphene," *Nano Res.*, vol. 1, no. 2, pp. 116–122, Aug. 2008.
[40] J. E. Fischer and T. E. Thompson, "Graphite intercalation compounds," *Phys. Today*, vol. 31, no. 7, pp. 36–45, Jul. 1978.
[41] M. S. Dresselhaus and G. Dresselhaus, "Intercalation compounds of graphite," *Adv. Phys.*, vol. 51, no. 1, pp. 1–186, Jan. 2002.
[42] J. Shioya, H. Matsubara, and S. Murakami, "Properties of AsF_5-intercalated vapor-grown graphite," *Synth. Met.*, vol. 14, no. 1/2, pp. 113–123, Mar. 1986.
[43] C. Xu, H. Li, and K. Banerjee, "Graphene nano-ribbon (GNR) interconnects: A genuine contender or a delusive dream?," in *IEDM Tech. Dig.*, Dec. 2008, pp. 201–204.
[44] *Intl. Tech. Roadmap for Semiconductors (ITRS)*, 2007. [Online]. Available: http://public.itrs.net
[45] S. Datta, *Electronic Transport in Mesoscopic Systems*. Cambridge, U.K.: Cambridge Univ. Press, 1995.
[46] C. T. White and T. N. Todorov, "Carbon nanotubes as long ballistic conductors," *Nature*, vol. 393, no. 6682, pp. 240–242, May 1998.
[47] J. Jiang, J. Dong, H. T. Yang, and D. Y. Xing, "Universal expression for localization length in metallic carbon nanotubes," *Phys. Rev. B, Condens. Matter*, vol. 64, no. 4, p. 045 409, Jul. 2001.
[48] H. Li, W.-Y. Yin, K. Banerjee, and J.-F. Mao, "Circuit modeling and performance analysis of multi-walled carbon nanotube interconnects," *IEEE Trans. Electron Devices*, vol. 55, no. 6, pp. 1328–1337, Jun. 2008.
[49] J. Hass, F. Varchon, J. E. Millán-Otoya, M. Sprinkle, N. Sharma, W. A. de Heer, C. Berger, P. N. First, L. Magaud, and E. H. Conrad, "Why multilayer graphene on 4H-SiC $(000\bar{1})$ behaves like a single sheet of graphene," *Phys. Rev. Lett.*, vol. 100, no. 12, p. 125 504, Mar. 2008.
[50] L. R. Hanlon, E. R. Falardeau, and J. E. Fischer, "Metallic reflectance of AsF_5-graphite intercalation compounds," *Solid State Commun.*, vol. 24, no. 5, pp. 377–381, Sep. 1977.
[51] W. Steinhogl, G. Steinlesberger, M. Perrin, G. Scheinbacher, G. Schindler, M. Traving, and M. Engelhardt, "Tungsten interconnects in the nano-scale regime," *Microelectron. Eng.*, vol. 82, no. 3/4, pp. 266–272, Dec. 2005.
[52] M. Traving, G. Schindler, and M. Engelhardt, "Damascene and subtractive processing of narrow tungsten lines: Resistivity and size effect," *J. Appl. Phys.*, vol. 100, no. 9, p. 094 325, Nov. 2006.
[53] X. Wang, Y. Ouyang, X. Li, H. Wang, J. Guo, and H. Dai, "Room-temperature all-semiconducting sub-10-nm graphene nanoribbon field-effect transistors," *Phys. Rev. Lett.*, vol. 100, no. 20, p. 206 803, May 2008.
[54] *Predictive Technology Model (PTM)*. [Online]. Avaialble: http://www.eas.asu.edu/~ptm/

Chuan Xu (S'08) received the B.S. degree in microelectronics and the M.S. degree in microelectronics and solid-state electronics from Peking University, Beijing, China, in 2004 and 2007, respectively. He is currently working toward the Ph.D. degree at Prof. Banerjee's Nanoelectronics Research Laboratory, Department of Electrical and Computer Engineering, University of California, Santa Barbara. During his M.S. degree, he worked on the fabrication and characterization of AlGaN/GaN heterostructure field-effect transistors.

During the summer of 2008, he was an Intern with the Electrical Interconnect and Packaging (EIP) Group, IBM T. J. Watson Research Center, Yorktown Heights, NY. His current research is focused on the modeling, design, and characterization of emerging interconnect materials, structures, and effects.

Mr. Xu was the recipient of the "2008 IBM Problem Solving Award Based on the Use of the EIP Tool Suite," which recognizes outstanding contributions by students in solving the most interesting problems using IBM's Electromagnetic Field Solver Suite of Tools called the EIP tools.

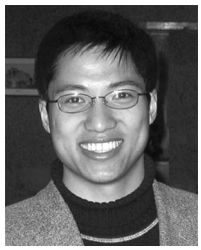

Hong Li (S'07) received the B.E. degree in electronic engineering from the Nanjing University of Aeronautics and Astronautics, Nanjing, China, in 2003 and the M.S. degree from the Shanghai Jiao Tong University, Shanghai, China, in 2008. He has been working toward the Ph.D. degree at Prof. Banerjee's Nanoelectronics Research Laboratory, Department of Electrical and Computer Engineering, University of California, Santa Barbara (UCSB), since 2007.

His research interests include the modeling and design of carbon nanomaterials for electronic applications, particularly VLSI interconnects and passive devices. Since December 2008, he has been the lead graduate student working on the development of a state-of-the-art carbon nanomaterial fabrication facility at UCSB's California NanoSystems Institute.

Mr. Li received a number of prizes for outstanding academic performance, including an Excellent Bachelor's Thesis Award during his undergraduate years.

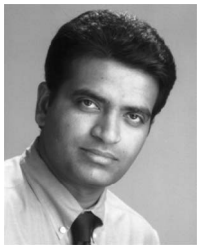

Kaustav Banerjee (S'92–M'99–SM'03) received the Ph.D. degree in electrical engineering and computer sciences from the University of California, Berkeley, in 1999.

In July 2002, he joined the Faculty of the Department of Electrical and Computer Engineering, University of California, Santa Barbara, where he has been a Full Professor since 2007. He is also an affiliated faculty at the California NanoSystems Institute (CNSI) at UCSB. From 1999 to 2001, he was a Research Associate with the Center for Integrated Systems, Stanford University, Stanford, CA. From February to August 2002, he was a Visiting Faculty with the Circuit Research Laboratories, Intel, Hillsboro, OR. He has also held summer/visiting positions at Texas Instruments Incorporated, Dallas, from 1993 to 1997, and the Swiss Federal Institute of Technology, Lausanne, Switzerland, in 2001. His research has been chronicled in over 170 journal and refereed international conference papers and in two book chapters on 3-D ICs. He is also a coeditor of the book *Emerging Nanoelectronics: Life With* and *After CMOS* (Springer, 2004). His current research interests include nanometer-scale issues in VLSI as well as circuits and systems issues in emerging nanoelectronics. He is also involved in exploring the design and fabrication of various nanomaterials for ultra energy-efficient electronics and energy harvesting/storage applications.

Prof. Banerjee received a number of awards in recognition of his work, including the Best Paper Award at the Design Automation Conference in 2001, the ACM SIGDA Outstanding New Faculty Award in 2004, the IEEE Micro Top Picks Award in 2006, and the IBM Faculty Award in 2008. He has served on the Technical Program Committees of several leading IEEE and ACM conferences, including the IEEE International Electron Devices Meeting, the Design Automation Conference, the International Conference on Computer Aided Design, and the International Reliability Physics Symposium. From 2005 to 2008, he served as a member of the Nanotechnology Committee of the IEEE Electron Devices Society. He has also served on the Organizing Committee of the International Symposium on Quality Electronic Design at various positions, including Technical Program Chair in 2002 and General Chair in 2005. Currently, he serves as a Distinguished Lecturer of the IEEE Electron Devices Society.